PAPER

Check for updates

Hydrogen *via* reforming aqueous ammonia and biomethane co-products of wastewater treatment: environmental and economic sustainability

Oliver Grasham,[*a] Valerie Dupont,[a] Timothy Cockerill,[a] Miller Alonso Camargo-Valero [b] and Martyn V. Twigg[c]

Green H_2 is increasingly viewed as a key energy carrier for the fight against climate change. Wastewater treatment plants (WWTPs) have the unique potential to be centres of renewable H_2 generation with the growing availability of two attractive feedstocks: biomethane and ammonia. An innovative and novel method of ammonia recovery from digestate liquor followed by a state-of-the-art H_2 production process named NWaste2H2 is demonstrated for a case-study WWTP. The recovered ammonia is used alongside biomethane for H_2 production and its diversion from conventional biological treatment has two other crucial benefits, with reductions in both associated electricity demand and emissions of nitrous oxide, an extremely potent greenhouse gas. Process modelling, supported by extensive experiments in a packed-bed reactor at bench-scale, demonstrate the prized capability of simultaneously performing steam methane reforming and ammonia decomposition to generate a H_2-rich syngas with yields close to equilibrium values. Greenhouse gas emission abatement from the replacement of diesel buses and reduced N_2O emissions from biological treatment could save up to 17.2 kg CO_2 equivalent (CO_2e) per year for each person served by the WWTP. An in-depth economic study illustrates the ability to achieve a positive net present value with a 10% discount factor as early as 5.8 years when the H_2 is prepared and sold to power fuel cell electric buses.

1 Introduction

Interest in the use of H_2 as an energy vector has made a significant resurgence in recent years. According to many in industry, government and academia, green H_2 has the potential to play an important part in the global transition to carbon-free economies.[1-4] There are numerous reasons, such as its ability to be used in existing infrastructure, carbon and pollution free emissions at use, historical utilisation in industry and its potential to penetrate all energy sectors (heat, power, transport and storage).[5] However, economically appealing methods of H_2 production from biogenic sources have been hard to come by,[6] something that may change with findings presented in this article.

Green H_2 can be produced by electrolysis of water using renewable electricity, steam methane/natural gas reforming (SMR) with carbon capture and storage (CCS), dark fermentation and biomass reforming and gasification.[7] H_2 generation *via* electrolysis from renewables and SMR with CCS are being touted as the most promising technology routes for significant

energy market penetration.[5] However, other generation methods should not be disregarded. One biogenic feedstock gaining interest is biogas from wastewater treatment plants (WWTPs), which can be steam reformed to produce H_2.[8-10] In the UK alone, WWTPs produce enough biogas to generate >1 TW h_{elec} each year,[11] proving it as a widely available potential H_2 source.

WWTPs also feature a hidden, largely unutilised hydrogen carrier in the form of ammonia. The liquor fraction of anaerobic digestate, which contains a considerable quantity of ammonia, is ordinarily recycled back into the treatment process. Air stripping-absorption is the most common method of ammonia recovery, with multiple companies providing commercially available products that are typically used to produce fertilisers.[12] Scarce examples of process modelling for ammonia recovery for generation of fertilisers exist, with Errico *et al.*[13] providing an almost stand-alone case. As of August 2020, the market value of fertiliser in the UK is at £0.2 per kg ammonium nitrate (£0.58 per kg N).[14] This makes it difficult for the recovery of ammonia from digestate liquor to be profitable. As such, this paper aims to highlight an alternative use for aqueous ammonia recovered from digestate which could be more attractive to wastewater treatment plant operators. At a market value of £4.50 per kg H_2 a conversion from ammonia could have a value of up to £0.81 per kg N.

[a]*School of Chemical and Process Engineering, The University of Leeds, LS2 9JT, UK. E-mail: O.R.Grasham@leeds.ac.uk*

[b]*School of Civil Engineering, The University of Leeds, LS2 9JT, UK*

[c]*Twigg Scientific and Technical Ltd, Caxton, Cambridge, CB23 3PQ, UK*

If recovered effectively in a highly pure stream (as opposed to a fertiliser), it could provide a top up of H_2 alongside that produced *via* the reforming of biogas/biomethane. Yet there is the potential to recover this ammonia and a potential use of it is to thermally crack it to form H_2 and nitrogen (eqn (11)). This was in some capacity demonstrated in a paper by Grasham *et al.*,[15] where the recovery of ammonia from digestate liquor at a case study WWTP was modelled along with its consequent use with bio-methane in a solid-oxide fuel cell for the generation of heat and power. Here, ammonia cracking and SMR occur within the SOFC to facilitate the cogeneration of heat and power.

A significant advantage of diverting ammonia from conventional treatment is the positive impact on a WWTP's energy consumption and emissions of greenhouse gases (GHGs). The release of ammoniacal and nitrate nitrogen at WWTPs is restricted under EU law[16,17] due to the damaging consequences of emitting ammonia and nitrates into aquatic ecosystems. The most popular method of achieving NH_3 conversion to N_2 is *via* biological nitrification and denitrification in a multi-stage activated sludge process (ASP). Unfortunately, the aerobic bacteria involved in nitrification require considerable amounts of oxygen to be pumped into tanks, increasing the WWTP's electricity consumption. Garrido *et al.*[18] calculated that 4.57 kW h of electrical energy are required for every kg of oxidised nitrogen.

A further noteworthy issue with nitrification–denitrification systems is the generation of nitrous oxide (N_2O) as an intermediary and side-product.[19] N_2O is a particularly potent GHG with a global warming potential (GWP) 298 times that of CO_2 over a 100 year period. The UK Water Industry Research Ltd suggest an emission factor of 0.002 kg of N in the form of N_2O ('N_2O–N') for every kg of nitrogen in the WWTP load.[20] Moreover, N_2O emissions from wastewater treatment are notoriously variable. For example, Kampschreur *et al.*[19] found N_2O emissions of 0–14.6% of the nitrogen load from a review of literature on emissions from full scale operational facilities. Meanwhile, Parravicini *et al.*[21] have developed a regression model for estimating N_2O emissions based on the destruction of nitrogen during conventional treatment. Regardless of the exact emission factor, diversion of ammonia found in digestate liquor from activated sludge treatment could significantly improve a facility's energy consumption and carbon footprint.

H_2 fuel cell electric buses have been identified as a notably attractive option to decrease carbon emissions from transport, whilst also improving urban air quality.[22,23] A recent report by the Hydrogen Council found that fuel cell buses were the most competitive way to decarbonise medium-long range bus travel.[24] According to the IEA, by the end of 2019 there were around 4600 fuel-cell electric buses globally.[25] Ten of these fuel cell buses are currently in use in Aberdeen, UK and have been praised for their influence in the city's recent emission reductions.[26] Hatch *et al.*[27] performed a techno-economic analysis of H_2 production scenarios at WWTPs as a fuel for bus transport, concluding that steam methane reforming (SMR) of bio-methane could be a cost-competitive option for decarbonising a fleet of buses. Furthermore, it showed that SMR was the most commercially attractive technology option when compared to alternatives including molten carbonate fuel cells (MCFCs) and wood gasification.

Given the current GHG emissions from diesel buses, a conversion to green H_2 could save almost 1.3 kg CO_2e per km.[28]

This work details the feasibility of innovatively combining ammonia recovery and H_2 production system at wastewater treatment plants in a process we named NWaste2H2, with the use of generated H_2 as a bus fleet transportation fuel. The pioneering system, which uses both ammonia catalytic decomposition and methane steam reforming to produce H_2 simultaneously, has been modelled and optimised using Aspen Plus® V.10.[29] A techno-economic study has been carried out to determine the financial feasibility and attractiveness of implementing the process at an operational WWTP in the UK. To the authors' knowledge this is the first instance of reporting the cumulative benefits of greenhouse gas emissions savings during green H_2 production by using a combination of both biogas and bio-ammonia feedstock, with a sizeable part of the savings being achieved by suppression of nitrous oxide emission from the main WWTP process. It is suggested that widespread process implementation, could provide an important contribution to global H_2 infrastructure with its economic competitiveness, whilst also reducing WWTP GHG emissions. The tangible viability of generating H_2 in the proposed format has been analysed *via* a unique experimental procedure combining steam methane reforming and ammonia decomposition carried out in a packed-bed reactor over a catalyst.

2   Methods for process analysis

A chemical process model was developed in Aspen Plus® V.10 (ref. 29) and sensitivity analysis was carried out to provide an energy efficient method of NH_3 recovery from a low concentration ammonia solution representative of digestate liquor. This was combined with a process simulation for H_2 generation *via* a combination of the catalytic processes of steam bio-methane reforming, water–gas-shift and bio-ammonia decomposition. A simplified process flow diagram of these steps can be found in Fig. 1 with a more detailed version in Fig. 3. The removal of CO_2 and H_2S from the biogas has not been modelled in Aspen Plus® but included in economic analysis as a high-pressure water scrubbing system. The following assumptions were also utilised throughout:

● Ambient conditions set at 1 bar, 23 °C.

● Air composition assumed 79 : 21 split of N_2 : O_2 only.

Biomethane and digestate liquor flows and liquor ammonia concentrations are based on data from a real WWTP serving a population equivalent to 750 000 people in the UK. Ammonia concentration of the digestate liquor was determined *via* analysis of 11 samples from the reference WWTP between October 2014 and May 2016 by members of the BioResource Systems Research Group at the University of Leeds. The 4500 N Standard Method as reported in ref. 30 was used for determination, detailing an average concentration of 1.5 g L^{-1}.

The WWTP's current energy usage stands at 60 MW h_{elec} per day and generates 40 MW h_{elec} per day *via* conventional cogeneration technology fuelled with biogas, thus operates with a net energetic deficit of 20 MW h_{elec} each day. Biomethane production of 8229 kg per day was back calculated from the
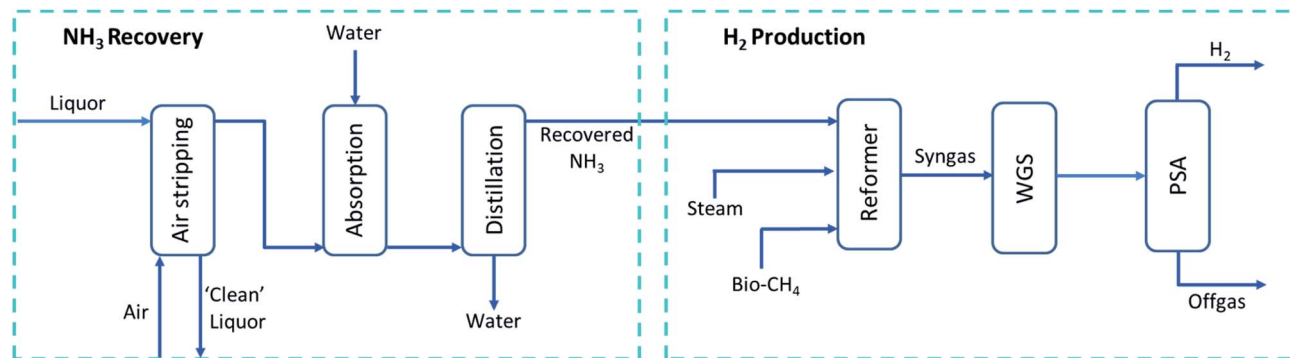
Fig. 1 Simplified process flow diagram (PFD) of process modelled using Aspen Plus®. Full PFD found in Fig. 3.

electricity generation based on a 35% electrical efficiency of the plant's combined heat and power CHP units (LHV basis). The WWTP can be considered 'large' in a UK context, producing 30% more power than the industry mean. Digestate liquor production of 661 m^3 per day was asserted from an equivalence of 0.63% of total wastewater inflow, interpreted from,[31] which stands at a daily average of 105 000 m^3 per day.

N$_2$O emission savings have been estimated by calculating an N$_2$O emission factor based on the regression model developed by Parravicini et al.[21] which estimates N$_2$O emissions based on the % removal of total nitrogen (TN) during treatment equation:

$$y = -0.049x + 4.553 \qquad (1)$$

where, x is the % removal of TN, calculated as the incoming flow of TN minus the TN contained in the final effluent and solid digestate. The referenced WWTP used throughout this study has a removal efficiency of 68.4%. Using eqn (1), this assigns an emission factor of 0.012 kg N$_2$O–N kg^{-1} TN$_{influent}$. For calculating the lifecycle emissions from any changes in grid electricity use, an emission factor of 107 g CO$_2$e per kW h has been used.[32] The H$_2$ generated in the process is speculated to be used as a fuel for fuel cell electric buses (FCEB), replacing their diesel counterparts. Accordingly, the CO$_2$ emission abatement has been calculated using current emission factors from the UK Department for Business, Energy and Industrial Strategy (BEIS).[33] In the BEIS report, the average local bus was calculated to emit 104.71 g CO$_2$e per passenger per km travelled. With an average occupancy of 12.24, this equates to 1.28 kg CO$_2$e per km travelled. Abated emissions associated with the use of the green H$_2$ generated in this proposed process were calculated based on kilometres travelled using the H$_2$ generated, where a FCEB uses 90 g H$_2$ per km.[26]

The GHG emission implications of process implementation were determined via eqn (2), where GHG$_{total}$ are the total savings GHG$_{NH3,diverted}$ are the savings facilitated by the diversion of ammonia from conventional biological treatment, GHG$_{bus,abatement}$ and GHG$_{grid,NG}$ are the abated emissions from converting diesel-buses to H$_2$, GHG$_{grid,elec}$ are the emissions arising from the increased use of grid electricity and heat that would other-wise have been met by the plant's CHP system, all in units of CO$_2$e, The grid-supplied power and heat have carbon intensities of 107 and 210 g CO$_2$ per kW h respectively.[34,35]

$$GHG_{total} = GHG_{NH_3,diverted} + GHG_{bus,abatement} - GHG_{grid,elec} - GHG_{grid,NG} \qquad (2)$$

3 Economic analysis methodology

The economic model developed in this work uses the aforementioned reference wastewater treatment plant as a case study for process implementation. The assumption was made that the CHP units have already returned their investment – making the facility open to alternative processing routes for the biogas generated. A net present value (NPV) analysis has been carried out to determine the financial robustness of process implementation (economic sustainability). NPV takes into account the time value of money, where the value of a sum of money is worth more in the present than the same sum of money will be worth in the future. Eqn (3) displays the calculation used for NPV:

$$NPV(i, N) = \sum_{t=0}^{N} \frac{R_t}{(1+i)^t} \qquad (3)$$

where; i is the discount rate (as a fraction), N is the plant lifetime, t is the year of operation and R_t is the net cash flow for the

Table 1 Economic analysis index

RPI (%)	2.87
H$_2$ fuel price (£)	4.50
RHI price (£ per kW h)	0.0116
Industry electricity price (£ per kW h$_{elec}$)	0.1055
Industry heat price (£ per kW h$_{th}$)	0.0233
Scaling factor	0.6
Discount rate (%)	10
Annual maintenance (3%)	3
Large-scale replacement costs after 5, 10, 15 years (% of CAPEX)	15, 50, 15
Catalyst cost (£ per kg H$_2$)	0.15
RTFO value (2018)	0.15
Employees/shift	3.8
Shifts/day	3
Personnel for 40 h week	17.2
Average salary (£)	37 500
Salary interest (%)	2.99

year. A discount factor of 10% has been used in this study meaning that when NPV turns positive, investors will have achieved a mean 10% annual return on their initial investment and the time it takes to achieve this can be labelled as the discounted payback period. A 10% discount factor may be considered as relatively high but was chosen to ensure no overestimation of the system's potential profitability. The discount factor is displayed in the economic analysis index (Table 1) alongside other important variables used in the financial analysis.

Most equipment and installation costs have been determined using Aspen Plus® Economic Analyzer (APEA).[36] The total installed costs which comprise the total CAPEX include: above ground piping, poling, concrete, instrumentation underground/above ground electrics, grout and labour costs. The National Renewable Energy Laboratory (NREL) have developed an economic model for a H_2 production system[37] with the inclusion of a H_2 refuelling station. The NREL model was utilised to determine the total installation costs of units where APEA could not be used accurately, and an exchange rate of £0.78/$ has been used throughout. The calculation displayed in eqn (4), known as the six-tenths factor rule, was used to estimate the required adjustment in costs according to the scale difference with the NREL model.

$$\text{Cost of equipment } a = \text{cost of equipment } bX^{0.6} \tag{4}$$

In eqn (4), cost of equipment a and b are the unknown and known unit cost respectively, X is the multiplication factor for the known capacity difference between unit a and unit b (a/b), 0.6 represent the 'scaling factor' often used to approximate scaling costs. This method of cost estimation was used for the primary reformer, the two water–gas shift ('WGS') reactors, the pressure swing adsorber unit (PSA) and the pre-PSA condenser. The NREL economic model also includes a compression storage and dispensing (CSD) part of the plant which is hypothesised to be for the use of H_2 powered buses. As such, the associated CSD costs detailed in the NREL model have been scaled for use in this body of work. The CSD system consists of the compression of generated H_2 to 350 bar, ready for dispensing to H_2-fuelled buses. The costing of the stripping gas pre-heater (AIRHT) has been estimated using the cost curve for a stainless steel direct fired heater as displayed in Peters et al. (pg. 692)[38] and adjusted for inflation via long term UK retail price index (RPI). RPI has also been used as the figure for year-on-year interest rate.

Catalyst costs have been proposed at $0.19 per kg of H_2 as detailed in Kaiwen et al.[39] for nickel-based catalyst. The cost target of renewable H_2 for transport has been stipulated by the European Union at £4.50 (€5) per kg, equivalent to the value discussed by Reuter et al.[40] whereby H_2 would be competitive with diesel-based bus transportation. This is further backed by the Hydrogen Council who state that H_2 could competitively supply 30% of all transport with a price at the pump of $6 per kg (£4.60 per kg).[24] Expenditure on heat has been calculated with a cost of 2.33 p per kW h as detailed in the BEIS report on gas and electricity prices in the UK non-domestic sector.[41] The required expenditure for heat has been determined using the

requirements of blocks AIRHT and DIST (displayed in Fig. 3) with a thermal transfer efficiency of 80%. This is required as the heat ready for export from the process is not of a high enough quality to meet the requirements of AIRHT and DIST. The electricity price has been set as the average for a 'large' power consumer in the UK at £10.58 pence per kW h.[41] The expenditure on electricity has been valued via the power consumption of each compressor and pump simulated in Aspen Plus® and the power requirement of CSD calculated from the NREL economic model. Replacement costs have been inferred from the aforementioned NREL economic model[37] whereby after five and fifteen years replacement costs equate to 15% of the initial capital investment and 50% after 10 years.

Cost of labour was calculated with the determination of required operators via data obtained by Alkhayat & Gerrard and described in Turton et al. as eqn (5).[42,43] The calculation can be found in eqn (5) where, N_{OL} is the number of operators per shift, P_P is the number of processing steps involving the handling of particulate solids and N_{np} is the number of non-particulate processing steps.

$$N_{OL} = (6.29 + 31.7P_P^2 + 0.23N_{np})^{0.5} \tag{5}$$

The renewable transport fuel obligation (RTFO) is the UK's chief policy for reducing GHG emissions in the transport sector. RTFO certificates are granted to producers of low carbon/renewable fuel which can then be traded in an open market to organisations that have not met their certificate obligation. Renewable H_2 is awarded 4.58 certificates per kg and a conservative market value of 15 p per certificate has been assigned in this study.[44]

Sensitivity analysis has been carried out to indicate which factors will play an important role in the overall feasibility of potential process integration. Figures for the H_2 selling price, overall annual expense, initial capital investment and catalyst cost have been altered by ±15% to demonstrate the possible impact on the systems overall profitability in NPV terms. This sensitivity analysis also provides an indication of the security of the system's potential profitability.

4 Experimental methods

The primary reformer developed in the process model described in this article provides the platform for both ammonia decomposition and steam methane reforming. To the authors' knowledge this simultaneous method of H_2 generation has not been tested in a packed-bed reactor using commercial grade catalysts. Therefore, the following experiments have been carried out to demonstrate the capability of 'co-reforming' methane and ammonia accordingly. Direct use of experimental data in the process model would be improper due to the disparity in thermodynamic conditions, notably that the reformer presented in the process model is running at a pressure of 25 bar compared to 1 atm experimentally. Nevertheless, by comparing the results to equilibrium equivalents it is possible to infer the validity of the data presented in the process model. Meanwhile experimental carbon deposition analysis was
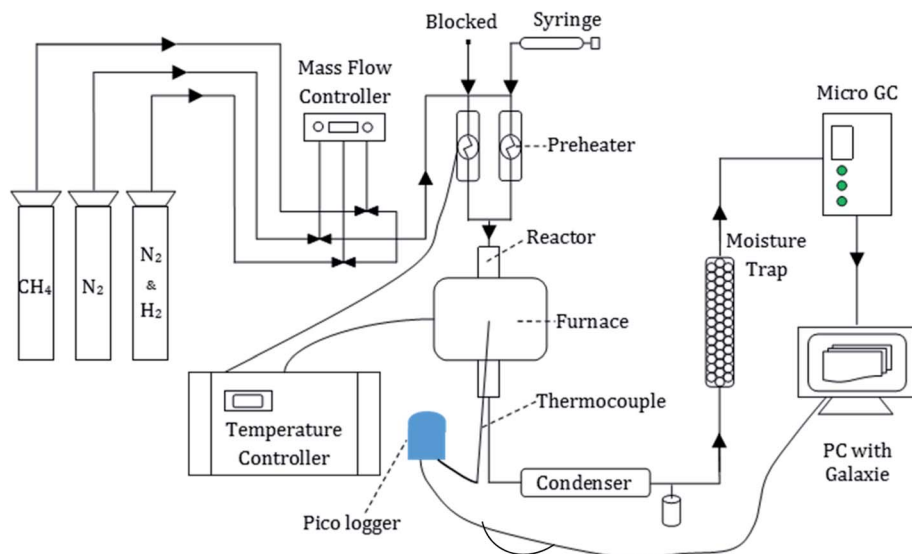
Fig. 2 Experimental H_2 production rig setup.

performed to highlight potential associated operational difficulties unidentified during equilibrium-based simulations.

Fig. 2 illustrates a schematic of the bench-scale rig used for the combined ammonia decomposition and steam methane reforming experiments. Three forms of compressed gases were connected to the rig: CH_4, N_2 and a 5 vol% H_2/95 vol% N_2 mix. The flow of the gases was controlled by MKS (US) mass flow controllers. The CH_4 flow represents biomethane from the WWTP, the N_2 was used as a carrier gas and the H_2/N_2 mix was used to reduce the catalyst from its original oxidised nickel state to the catalytically active metallic Ni. The gases were passed through electrical pre-heaters before entrance into the reactor. Liquid feedstock (de-ionised water and/or aqueous ammonia solution) was supplied to the system *via* a 20 ml BD Plastipak syringe with a stainless steel Luer lock needle *via* a New Era (US) Pump System Inc (model NE-1000). The ammonia solution used was a 25 wt% ammonia solution from Fischer Scientific (US). The liquid feed passed through a preheater set at 150 °C to vaporise before entrance to the reactor. Heating tape was used to aid the maintenance of temperature between the base of the preheaters and the reactor. Much of the rig was insulated to prevent thermal losses as much as possible.

The reactor was made of a 316 stainless steel tube with an internal diameter of 9.8 mm and positioned inside an electric tube furnace (Elite Thermal Systems TSV10/20/85) which provided the resistive heating to reach the desired reactor temperature. The internal temperature was monitored *via* a thermocouple connected to a pico-logger console in communication with a PC. The thermocouple reached roughly half way up the tube and provided a support in which a bed of 4 μm mean diameter quartz wool sat. The quartz wool, in turn, provided a semi-permeable and non-reactive platform in which the powder catalyst could sit. A commercial grade 18 wt% NiO/α-Al$_2$O$_3$ catalyst from Twigg Scientific & Technical Ltd (UK) was crushed and sieved to a diameter between 150–250 μm for use in each experiment.

The outlet from the reactor was fed into a stainless steel condenser which cooled the product gas using a counter-flow of (30 vol%) ethylene glycol/(70 vol%) water cooling liquid at −2 °C. A stainless steel condensate trap was located after the condenser and could be detached in order to remove, store and later analyse any condensate generated. Downstream of the condenser, a stainless steel moisture trap, filled with silica gel beads, facilitated the removal of all moisture from the syngas to ensure only a dry gas entered the micro gas chromatograph (GC).

The Varian (US) CP 4900 micro GC provided compositional analysis of the dry product gas from the reactor. It contained two thermal conductivity detectors (TCD) and two columns. The first was a Molecular Sieve 5A plot column and was calibrated to detect the following gases: H_2, O_2, N_2, CH_4 and CO. The second was a Pora Plot Q column which was calibrated for measurement of CO_2, CH_4, C_2H_6, C_2H_4, C_3H_8 and C_3H_6 gas concentrations. Argon was used as its carrier for both columns in the Varian micro GC module.

Carbon deposition on the catalyst was determined using CHN analysis Thermo Scientific (US) Flash 2000 Elemental Analyzer. The ammoniacal nitrogen remaining in the condensate was determined using a Hach (US) AP3900 Laboratory Robot with Hach LCK 303 ammonium calorimetry cuvettes. It was found that over time the ammonia contained in the aqueous solution volatilised during sample preparation. This meant that the intended S : C ratios were adjusted for actual S : C achieved in the reactor after analysis for comparison with equilibrium modelling. Equilibrium modelling was carried out using an RGibbs reactor in Aspen Plus® with identical inlet flows to the experiments so that comparisons between the two datasets could be made.

N_2 was used as the carrier gas through the rig but was also formed during the decomposition of ammonia. Ordinarily the known quantity of N_2 outlet would be used as a reference to calculate the molar flows of the other gases used in the syngas.

However, without knowledge of the extent of ammonia decomposition occurring, an alternative method of product flow analysis was necessary. Therefore, a 'contribution analysis' approach was taken whereby speculative amounts of ammonia decomposition were considered until the composition of the syngas matched that of the micro-GC output.

This was performed *via* eqn (6)–(8). Eqn (6) describes *via* a N elemental balance, how the molar flow of any specie x from the reactor ($\dot{n}_{x(\text{out})}$) can be calculated using the known molar flows of N_2 into the reactor ($\dot{n}_{N_2(\text{in})}$), the N_2 generated from ammonia decomposition, the mole fraction of N_2 ($y_{N_2(\text{out})}$) and the mole fraction ($y_{x(\text{out})}$) of specie x measured in the product gas. Potential ammonia conversion *via* decomposition was iteratively altered between 5 and 100% to provide hypothetical specie molar flows through eqn (6). Stoichiometry dictates that for each mole of CO generated ($\dot{n}_{CO}$) *via* SMR (reaction (9)) there would be three moles of H_2. Similarly for every mole of CO_2 generated ($\dot{n}_{CO_2}$) *via* WGS (reaction (10)) there are 4 moles of H_2. This provided the basis for eqn (7) which describes the production of H_2 from the combined SMR and WGS reactions ($\dot{n}_{H_2(\text{contribution})}$). Eqn (7) was performed for runs with and without ammonia present, as it enables calculation of the difference in H_2 flows from the reactor *via* SMR and WGS ($\Delta\dot{n}_{H_2(\text{contribution})}$). When this is taken from the measured difference in H_2 flows from the reactor ($\Delta\dot{n}_{H_2(\text{out})}$) it was then possible to calculate the H_2 provided solely by ammonia decomposition ($\dot{n}_{H_2(NH_3\text{decomp})}$). During ammonia decomposition (reaction 11), for every mole of N_2 generated, 3 moles of H_2 are produced. As such, the true $\dot{n}_{H_2(NH_3\text{decomp})}$ was determined by iteration from the ammonia decomposition sensitivity analysis when it equalled three times that of $\Delta\dot{n}_{N_2(\text{out})}$. True $\Delta\dot{n}_{H_2(NH_3\text{decomp})}$ value was then used to determine the percent ammonia conversion reported in the results.

$$\dot{n}_{x(\text{out})} = \left(\frac{\dot{n}_{N_2(\text{in})} + \dot{n}_{N_2(\text{speculative NH}_3 \text{ decomp})}}{y_{N_2(\text{out})}} \right) \times y_{x(\text{out})} \sqrt{b^2 - 4ac} \tag{6}$$

$$\dot{n}_{H_2(\text{contribution})} = 3\dot{n}_{CO} + 4\dot{n}_{CO_2} \tag{7}$$

$$\dot{n}_{H_2(NH_3\text{decomp})} = \Delta\dot{n}_{H_2(\text{out})} - \Delta\dot{n}_{H_2(\text{contribution})} \tag{8}$$

Runs with and without ammonia were completed at temperatures 700 °C, 750 °C and 800 °C and at S : C ratios close to S : C ratios approximating the intended 2, 3 and 4 (precision adjusted afterwards). A constant weight hourly space velocity (WHSV = total mass flow rate divided by reactor bed mass load) of 2 h^{-1} was used in each experiment. The gas hourly space velocity (GHSV = total volumetric flow rate dived by volume of catalyst bed) varied between 4014 and 4234 h^{-1}. Total experimental run time averaged at 3 hours which generated 50 data points from the micro-GC, providing enough time for robust analysis of the mean syngas composition and the extent of carbon deposition. Experimental feed compositions can be found in Table 7. Each condition was tested in duplicate and the runs with the least variability used for analysis.

5 Simulation setup and NWaste2H2 process operation description

Aspen Plus® V.10 was used to simulate the novel H_2 production process. An "ENRTL-RK" (Electrolyte Non-Random Two Liquid with Redlich-Kwong) base method were used throughout. Fig. 3 displays the full chemical processing plant as designed for this study. The ammonia recovery process is as that detailed in Grasham *et al.*[15] with the exception that the flash separation unit was replaced with a distillation column. The air stripper
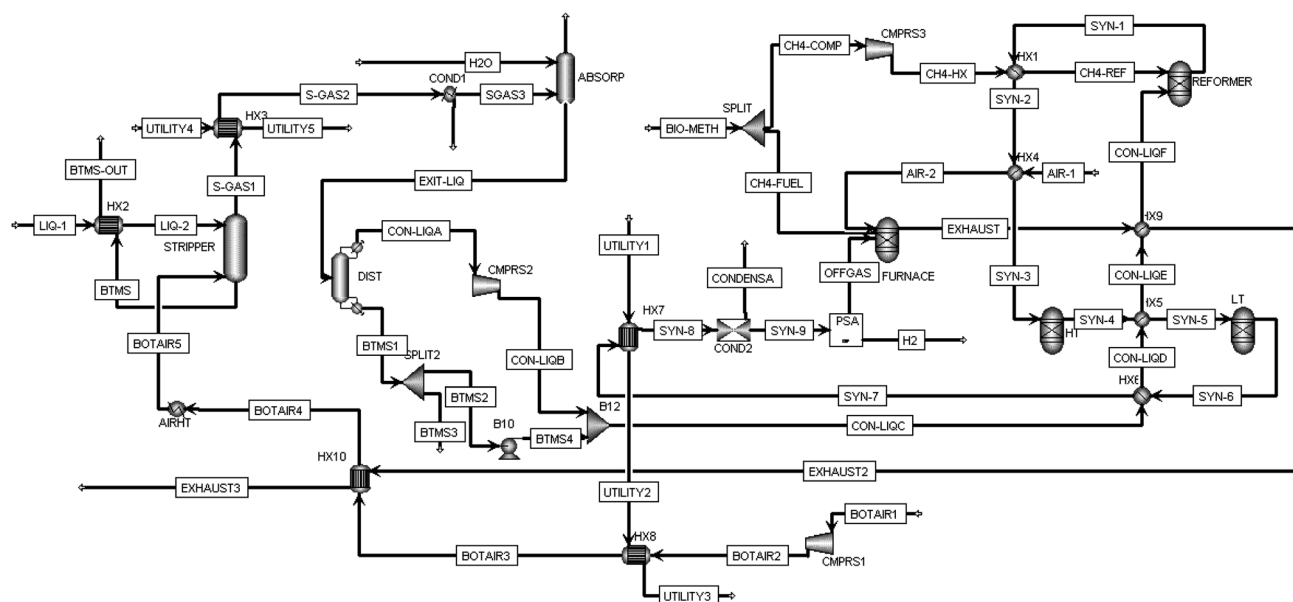

Fig. 3 Process flow diagram of ammonia recovery and H_2 production NWaste2H2 system (without CSD).
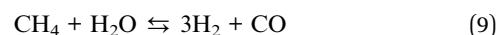
was simulated using a RadFrac column with 30 trays, no condenser or reboiler, 'standard' convergence and using equilibrium (rather than rate-based) calculations. It is presumed that the digestate liquor has been treated with NaOH to increase the pH to a state in which all ammonia is contained in its free (NH_3) form rather than as ionic ammonium. The recovery process begins with the introduction of digestate liquor (LIQ-1) which is preheated by exchange with the bottoms' exit from the stripper (STRIPPER). LIQ-2 then enters the top of the stripper ('above stage 1'). Stripping air is compressed to 1.3 bar, preheated *via* two heat exchangers and a heater to 500 °C and fed to the bottom ('on stage 30') of the stripper. A 10% pressure drop was simulated through the stripping column.

The ammonia is desorbed and released with air and a small amount of water vapour. This stream is cooled, allowing water to condense before entering an absorption column (ABSORB). The absorption column has also been simulated using a RadFrac column with 10 stages, no condenser or reboiler, using 'standard' convergence and equilibrium calculations. Here, a counter-flow stream of water (entering the top of the column above stage 1) meets the stripped material (entering the bottom of the column on stage 10) which allows the 'recapturing' of ammonia, leaving at the base of the absorber. This stream (EXIT-LIQ) is then fed into the distillation column (DIST) with 15 stages, a 'partial-vapour' condenser, kettle reboiler, using standard convergence and equilibrium calculations. The gaseous outlet from the distiller (CON-LIQA), containing a highly concentrated ammonia mixture is to be prepared for H_2 production. The recovered ammonia stream is pressurised to 31 bar before mixing with a fraction of the distillation bottoms (BTMS2), the quantity of which is dictated by a pre-determined feed molar steam to carbon ratio (S : C) in the reformer, for which the carbon is from the biomethane co-feed. This combined stream, (CON-LIQC) is heated *via* a number of heat exchangers (HX6, HX5 and HX9) before entering the primary reformer/cracker (REFORMER) at 25 bar.

The reformer is simulated with an RGibbs reactor where the minimisation of Gibbs free energy is used to calculate the product yields and heat demand. Here, the pressurised recovered ammonia stream is met with pressurised and pre-heated bio-methane. At 1000 °C, the reformer generates a syngas formed primarily by a mixture of reactions (9–11). Reaction (9) describes 'steam methane reforming' (SMR) whereby methane is converted to H_2 gas and carbon monoxide using high temperature steam. Reaction 10 displays 'water gas shift' (WGS) where steam is used to convert carbon monoxide to H_2 gas and carbon dioxide. Reaction 11 exhibits the thermal decomposition/cracking of ammonia to H_2 and nitrogen gas. S : C of 2, 3 and 4 were analysed in this work to determine the most advantageous conditions from both efficiency and economic points of view. S : C can be described as the molar ratio of H_2O and CH_4 entering the reformer.

The syngas produced from the primary reformer (SYN-1) expends heat *via* transfer with the reformer and furnace inlets in heat exchangers 'HX1' and 'HX4'. It enters the high temperature shift HT-WGS (HT) and low temperature shift LT-WGS

reactors (LT), also represented as RGibbs reactors, at 350 °C and 205 °C inlet temperatures respectively, for maximum CO conversion to CO_2 and concurrent production of H_2 from the water co-reactant *via* reaction (5). Each shift reactor operates adiabatically, so the exothermic nature of the WGS reaction creates a moderate temperature hike in each reactor. The syngas is then cooled and dried before a PSA unit generates a pure H_2 product containing 90% of the H_2 present in the PSA inlet.

$$CH_4 + H_2O \leftrightarrows 3H_2 + CO \tag{9}$$

$$CO + H_2O \leftrightarrows H_2 + CO_2 \tag{10}$$

$$2NH_3 \leftrightarrows 3H_2 + N_2 \tag{11}$$

A furnace was used to generate heat for the process. It was simulated *via* an 'RGibbs' reactor (FURNACE) and is fuelled by a portion of the AD-biomethane product *via* the stream 'CH₄-FUEL' together with any remaining H_2, CH_4 and CO present in the PSA's offgas (OFFGAS). The quantity of biomethane fed to the furnace is determined *via* a 'Design Specification' block which stipulates that the flow of methane should facilitate a post-reformer exhaust temperature of 1100 °C. The furnace then generates an excess of heat (heat duty) that equates to 110% of the reformer requirements. This fulfils the heat demand of the reformer and accounts for 10% thermal losses. A 10% pressure drop is experienced in each of the heat exchangers and reactors where the inlet pressure is slightly greater than atmospheric. Streams 'EXHAUST3', 'UTILITY3' and 'UTILITY5' shown in Fig. 3 provide the potential for heat export from the system. Their potential heat production have been calculated by cooling them to 23 °C and 1 bar *via* heater blocks in Aspen Plus® and given a 90% transfer efficiency factor.

A number of calculator blocks have been installed to the process model in order to fulfil associated process requirements, as detailed in eqn (12)–(15). Eqn (12) describes the requirement of an oxygen feed to the furnace to be 1.1 times that of the stoichiometric requirement. Eqn (13) is used to ensure that the ratio of nitrogen and oxygen in the air inlet remains at 79 : 21 on a molar basis. Eqn (14) ensures that the quantity of water entering as steam the primary reformer equates to the chosen steam to carbon ratio (S : C). Eqn (15) was used to simulate the losses of heat (10%) from the furnace to the reformer. Amongst these equations:$\dot{n}_{x,y}$ describes the molar flow of species 'y' in stream 'x' and $HD_{FURNACE}$ and $HD_{REFORMER}$ are the heat duties of the furnace and reformer respectively.

$$\dot{n}_{AIR\text{-}1,O_2} = 1.1$$
$$\times \left(\frac{\dot{n}_{OFFGAS,H_2} + \dot{n}_{OFFGAS,CO}}{2} + 2\left(\dot{n}_{OFFGAS,CH_4} + \dot{n}_{CH_4\text{-}FUEL,CH_4}\right) \right) \tag{12}$$

$$\dot{n}_{AIR-1,N_2} = \dot{n}_{AIR-1,O_2} \times 3.792 \tag{13}$$

$$\dot{n}_{BTMS2,H_2O} = (S:C) \times \dot{n}_{CH_4-COMP,CH_4} \tag{14}$$

$$HD_{FURNACE} = -1.1 \times HD_{REFORMER} \tag{15}$$

6 NWaste2H2 process modelling results

6.1 Ammonia recovery

The ammonia recovery process showcased in this body of work closely resembles that exhibited in Grasham et al.[15] However, as aforementioned, the flash separator has been replaced with a distillation column as sensitivity analysis proved a comparative energetic preference for distillation. Sensitivity analysis also demonstrated an energetic system preference for relatively low air flow rates at high temperatures for the air stripper (STRIPPER). This means an incoming air flow rate to the stripping in BOTAIR5 of 250 kmol h^{-1} (7213 kg h^{-1}) at 550 °C and 1.1 bar. The liquor has ammonia and water flow rates of 2.95 kmol h^{-1} and 1528.6 kmol h^{-1} (50.3 and 27 537.4 kg h^{-1}) respectively, and is preheated to 64.1 °C via exchange with the stripper's bottom exit before entering the top of the stripper, thus facilitating an average column temperature of 64.3 °C. The result of these air stripping conditions is the recovery of 91.8% of the ammonia held in the initial digestate liquor.

For the absorption step, a 145.5 kmol h^{-1} (3242.8 kg h^{-1}) flow of water has been used, enabling the recovery of 98.4% of the ammonia entering the column. This translates to 90.3% of the digestate liquor's ammonia. This means the bottom exit of the absorber (EXIT-LIQ) contains 173.8 kmol h^{-1} of H$_2$O and 2.67 kmol h^{-1} of NH$_3$. The distillation column demonstrates only minimal losses, recovering 99.5% of the ammonia from the absorption outlet. Combined, the ammonia recovery system showcased an ability to recover 89.9% of the ammonia held in the digestate liquor, equating to 2.65 kmol h^{-1} (45.2 kg h^{-1}). This is a considerable improvement on the 82% recovery potential demonstrated from the recovery process discussed in Grasham et al.[15] Fig. 4 illustrates the recovery and losses through each ammonia recovery step.

Any aqueous ammonia 'losses' via the stripper and distillation phases, as displayed in Fig. 4, will be diverted for conventional wastewater treatment with the rest of the digestate liquor. Gaseous ammonia is 'lost' during absorption in very small concentrations via a stream mainly consisting of air. This air can be used to supply the oxygen feed required in the WWTP's activated sludge process. These measures ensure there are no gaseous discharges of ammonia to the atmosphere and that any ammonia not undergoing reforming undergoes biological treatment.

6.2 H$_2$ production

The flow of key syngas species from the primary reformer under S:C conditions 2, 3 and 4 can be seen in Fig. 5. The most visible result present in Fig. 5 is the positive correlation between S:C and H$_2$ generation. This occurs due to Le Chatelier's principle whereby steam excess tips the SMR and WGS equilibria forward (reactions (9) and (10)), resulting in greater conversions of CO and CH$_4$, and leaving lower quantities of these species in the syngas. The conversions of methane in the reformer were found to be 94.8, 97.9 and 98.9% for S:C 2, 3 and 4 respectively. Meanwhile, the conversions of CO were 16, 25.2 and 32.6% for S:C 2, 3 and 4 respectively. The conversion of ammonia in each S:C scenario showed very little variability, lying between 99.24–
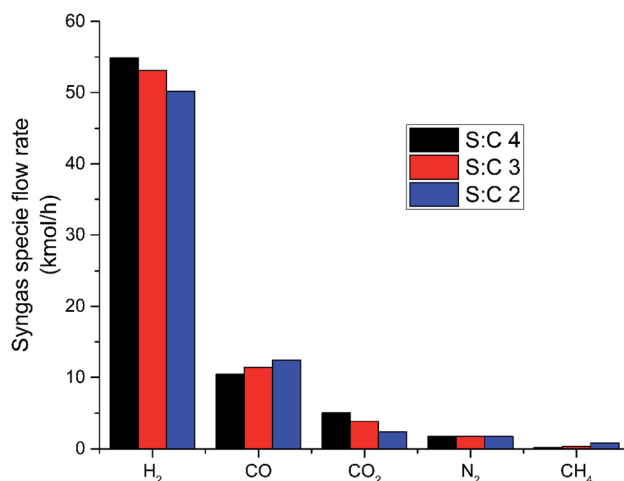

Fig. 5 Flow rate of key syngas species from the primary reformer for S:C 2, 3 and 4 scenarios at 25 bar and 1000 °C.
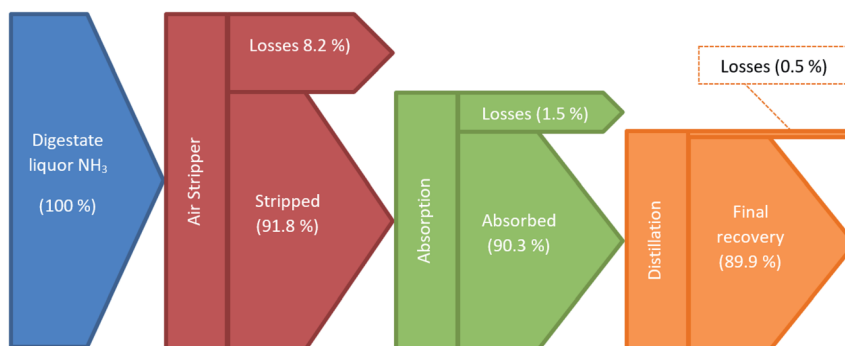

Fig. 4 Ammonia transfer route through recovery process.

99.45%. This high conversion was expected due to the high temperature (1000 °C) being used in the reformer.

The lower temperatures of the WGS reactors facilitate further conversion of CO *via* reaction 10. The HT-WGS reactor converts 51, 67 and 77% of the CO entering the reactor for S : C scenarios 2, 3 and 4 respectively. The LT-WGS reactor sees conversions of 66, 86 and 91% of the CO entering the reactor downstream of the HT-WGS. Again, this positive correlation can be attributed to the excess steam tipping the equilibrium of the WGS reaction towards the products. The effect of this is the generation of an additional 10.3, 10.8 and 10.1 kmol h^{-1} of H_2 for S : C scenarios 2, 3 and 4 respectively. This indicates that although CO conversion percentages improved with higher S : C ratio, the actual H_2 increase was fairly constant due to the greater inlet of CO from the primary reformer under lower S : C scenarios.

Fig. 6 highlights the impact of the WGS reactors on the composition of the syngas when compared to Fig. 5. CO has been significantly reduced, whilst CO_2 and H_2 have increased. The flows of H_2 from the LT-WGS reactor in stream SYN-6 were 60.6, 64.0 and 65.1 kmol h^{-1} for S : C 2, 3 and 4 scenarios respectively. The outlet from the LT-WGS reactor is removed of most of its water content before entering the PSA which recovers 90% of the H_2 contained in the syngas corresponding to 54.5 kmol h^{-1} (109.9 kg h^{-1}), 57.6 kmol h^{-1} (116.1 kg h^{-1}) and 58.6 kmol h^{-1} (118.1 kg h^{-1}) for S : C 2, 3 and 4 scenarios respectively.

6.3 Energetic implications

6.3.1 Heat. Although the H_2 gas production rates are superior with greater S : C ratios, the thermal demand for the reformer is more pronounced due to the higher volume of reactants requiring heating to maintain reactor temperature. This means that there is less heat to be recuperated in the upstream ammonia recovery. The heat demand of the AIRHT heater block, bringing air for stripping up to temperature, can be used as an indicator for how much heat is left after the H_2 production. Table 2 details the heat demand for AIRHT under
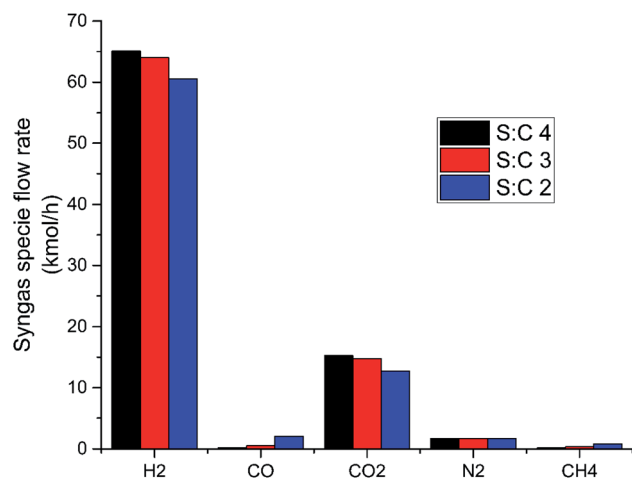

Fig. 6 Flow rate of key syngas species from the LT-WGS reactor for S : C 2, 3 and 4.

Table 2 System heat demand (negative numbers) and production (positive numbers) in kW$_{th}$. Stream temperatures shown in brackets

	S : C 2	S : C 3	S : C 4
Blocks			
AIRHT	−296.1	−615.0	−781.0
DIST	−365.5	−365.5	−365.5
Streams			
EXHAUST3	286.8 (125 °C)	298.5 (146 °C)	295.2 (148 °C)
UTILITY3	190.0 (57 °C)	293.4 (75 °C)	408.9 (95 °C)
UTILITY5	861.8 (63 °C)	861.8 (63 °C)	861.8 (63 °C)
Net total	677.0	473.2	419.3

Table 3 Temperature of each stream available from the process model for heat recovery at the wastewater treatment facility

	EXHAUST3 (°C)	UTILITY3 (°C)	UTILITY5 (°C)
S : C 2	65	125	63
S : C 3	88	146	63
S : C 4	120	148	63

each S : C scenario. It demonstrates that its energy requirement under the S : C 4 scenario is more than 2.5 times than under the S : C 2 scenario.

Table 2 also lists the heat demand of the distillation column's reboiler (365.5 kW$_{th}$) and of the process streams that could be used as sources (EXHAST3, UTILITY3 AND UTILITY5). Although each of these streams were found to contain a considerable amount of thermal energy providing positive net thermal power figures, this heat is of low quality in each case, as displayed in Table 3. None of these streams are adequate to meet the high temperature requirements of the air stripper's inlet. This must therefore be met from external sources, which adds to the comparative attractiveness of using lower S : C ratios used for reforming – from both energetic and economic vantage points. Although of low quality, the heat streams can be used on-site for purposes such as space-heating and anaerobic digestion.

6.3.2 Power. Table 4 exhibits the various consumers of electricity occurring with process integration, alongside the abatement enabled *via* the diversion of ammonia from conventional wastewater treatment for each S : C scenario. A positive correlation between S : C ratio and additional power requirements from process implementation can be seen. The

Table 4 Daily power consumption (+) and savings (−) in kW h with process integration to the reference wastewater treatment plant

	S : C 2	S : C 3	S : C 4
NWaste2H2 process	3890	3907	3930
Biogas clean up	5239	5239	5239
CSD	19 823	20 942	21 298
N-diversion	−4120	−4120	−4120
Net power use	24 832	25 968	26 347

key component of this audit is the electricity that would be needed for H_2 product preparation during compression, storage and dispensing (CSD). The reason for this is that H_2 would be pressurised to 350 bar for effective refuelling of high pressure tanks on-board the proposed fuel cell electric buses using the station. The CSD-derived power demand makes up over half of the additional power demand associated with the proposed process implementation.

The impact on electricity use from the diversion of digestate liquor ammonia can also be seen in Table 4. By diverting and utilising this ammonia, additional energy requirements of process implementation could be reduced by over 20% within each S : C ratio scenario. Nonetheless this is not enough to offset all of the energy needs that would come with process implementation. Accordingly, when adding the net power consumption figures displayed in Table 4, the referenced WWTP transforms from using an average 60 MWh$_{elec}$ per day to 84.8, 86 and 86.3 MW h pet day under S : C 2, 3 and 4 scenarios respectively.

6.4 Greenhouse gas emission savings

There are two ways in which the operation of the process would release lifecycle GHG emissions, being the use of high-quality heat from natural gas and increased grid electricity consumption. Conversely, there are two methods that would lessen the lifecycle GHG footprint of the wastewater treatment facility; the diversion of ammonia present in digestate liquor from its conventional treatment process and abated emissions from diesel buses replaced with H_2 fuel cell alternatives.

Table 5 indicates that impressive lifecycle GHG emission reductions would be possible with process implementation under each S : C scenario. It should be noted that these figures have been calculated with the assumption that there is no longer CHP technology in place at the WWTP. Abatement of air pollutant emissions *via* replacement of diesel-fuelled buses with H_2 fuel cell alternatives would have the greatest impact on the overall environmental attractiveness of process implementation. These GHG savings are directly related to the production of H_2 and is therefore more pronounced with higher S : C ratio utilisation in the process, as shown in Table 5.

The amount of high-quality heat required to perform effective air stripping and distillation was found to have a significant impact on reducing GHG emissions during process operation. The emissions resulting from the demand of high-quality heat under S : C 4 conditions outweigh the additional lifecycle

emission reductions experienced *via* abated bus transport emissions when compared to the S : C 3 scenario. This results in final GHG emission reductions of 35.20 tonnes CO_2e per day under the S : C 3 scenario which is 219 kg less than under S : C 4 conditions. The S : C 2 scenario demonstrated the lowest life-cycle GHG emission reductions but just 1 kg CO_2 per day less than under S : C 3 conditions. For each person served by the facility, or population equivalent (PE), the total GHG savings found in Table 5 equate to 17.1, 17.1 and 17.2 kg CO_2 per yr per PE for S : C 2, 3 and 4 conditions respectively.

6.5 Economic sustainability assessment of NWaste2H2

The total initial capital investment requirements CAPEX, which includes equipment capital and installation costs for process implementation were found to be £12.53 million ($16.06 million), £13.01 million ($16.68 million) and £13.29 million ($17.04 million) for S : C 2, 3 and 4 scenarios respectively. The breakdown under the S : C 3 scenario can be found in Table 6. The inter-scenario differences can mainly be attributed to the larger volume requirements of compression equipment under greater S : C conditions. In each case roughly 41% of the initial investment was accredited to the fuel preparation compression, storage and dispensing (CSD) systems; costing £5.21 million, £5.35 million and £5.40 million for S : C 2, 3 and 4 scenarios respectively. The greatest single unit investment cost from the discussed Aspen Plus® process was found to be CMPRS2 at £990 054.

Fig. 7 displays the NPV of the discussed process over its projected 20 year lifetime for the S : C 3 scenario. It demonstrates a discounted return on investment (*i.e.* when NPV equals 0) in 5.80 years which was the shortest of each S : C scenario considered. The equivalent length of time under S : C 2 and 4 conditions were 6.13 and 5.96 respectively. This means that investors will see an average 10% annual return on their investment in under 6 years from its opening day for two of the three S : C scenarios. At a projected H_2 value of £4.50 per kg, the associated (first year) income from H_2 sales only would stand at £4.33 million, £4.58 million and £4.65 million for S : C

Table 5 GHG emission sources from process implementation in kg CO_2e per day

	S : C 2	S : C 3	S : C 4
Net electricity	2657	2779	2819
High quality heat	3335	4942	5779
NH_3 diversion	−3222	−3222	−3222
Abated bus emissions	−37 964	−39 693	−40 790
Total	−35 194	−35 195	−35 414

Table 6 Installed capital costs under S : C 3 scenario

| Equipment	Installed cost (£)	Equipment	Installed cost (£)
C&S	5 347 789	PSA	172 225
CMPRS2	990 054	HX4	110 526
CMPRS3	988 416	COND1	84 942
Gas clean up	933 688	HX5	83 304
CMPRS1	577 902	HX10	82 758
REFORMER	552 690	COND2	73 491
AIRHT	544 076	HX7	58 734
HT	458 842	B10	57 486
LT	458 842	HX8	49 374
STRIPPER	348 348	HX9	48 582
DIST	306 072	HX6	44 694
HX3	204 126	HX1	27 462
HX2	200 382	FURNACE	25 855
ABSORP	180 726		
Total			13 011 386
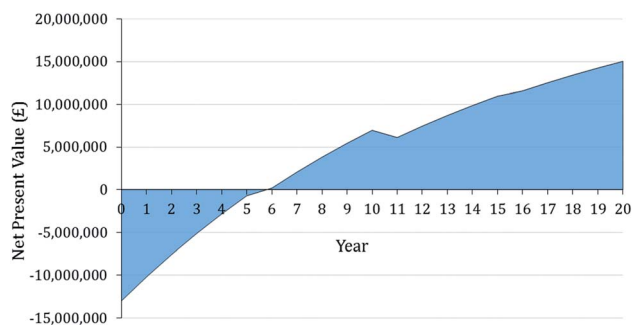
Fig. 7 Results of net present value over the 20 year lifetime of the novel H$_2$ production plant under S : C 3 conditions.

scenarios 2, 3 and 4 respectively. The sale of H$_2$ as a transportation fuel is by far the greatest revenue stream, comprising roughly 84% of the income possible from process implementation. The rest of the income is made up of RTFO certificate sales (~13%) and RHI (renewable heating incentive) payments (~3%).

Fig. 8 illustrates the first-year operational costs (OPEX) after implementation of the system under S : C 3 conditions. It can be noted that the greatest expenditure is on grid electricity for the various power requirements at £1.16 million a year,

equating to 46% of the total OPEX. Of spending on electricity, over two thirds can be attributed to the operation of the compression, storage and dispensing system. Whereas, the power requirements of the NWaste2H2 process (Fig. 3) contributes just 13% to the expenditure on grid electricity. The first year OPEX was found to be lowest in the S : C 2 scenario and highest in the S : C 4 scenario at £2.20 million, £2.34 million and £2.40 million for S : C scenarios 2, 3 and 4 respectively.

After the 20 year lifetime of the plant, the implications of the yearly income and OPEX data is that the S : C 3 scenario proved to be the most profitable of each scenario analysed. With final (20 years) NPV figures £14.08 million, £15.02 million and £15.00 million under S : C 2, 3 and 4 conditions respectively. This demonstrates that the low OPEX of the S : C 2 scenario would not outweigh the lower income potential, whilst the higher income potential of the S : C 4 scenario would not outweigh its greater OPEX. For these reasons it would be suggested that the plant use an S : C ratio of 3 in the primary reformer if the process was to be implemented at the reference WWTP.

Sensitivity analysis has been carried out on the economic study for the S : C 3 scenario, to highlight factors that would considerably influence the profitability of implementation and operation. This sensitivity has been done for due diligence purposes. For example, variations in these economic parameters could occur if some costs have been heavily under/ overestimated or severe weather occurs during construction or operation creating a spike in installation and operating costs. The results of the sensitivity analysis are displayed in Fig. 9. The tornado diagram demonstrates that a change in the price of catalyst would have minimal effect on the overall profitability with the implementation of the process at the reference WWTP, whilst a change in the market value of H$_2$ would impact significantly the system's profitability.

By decreasing the market value of H$_2$ by 15%, the NPV after 20 years would be 47% lower. This is noteworthy considering the strong uncertainty in the future price of green H$_2$. However, even with a 15% drop in its market value, a positive NPV (or discounted payback) could still be achieved in year 9 of operation and finish with an end-of-life NPV of +£7.9 million.

The H$_2$ price detailed in this report is that of the 'target price' set by Reuter et al.[40] for competitiveness with diesel rather than
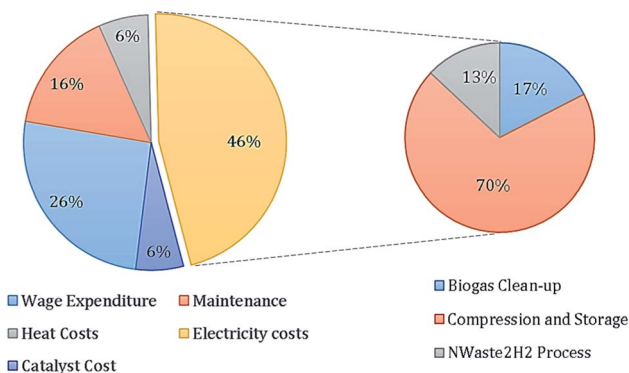

Fig. 8 Breakdown of first year OPEX for S : C 3 scenario with a further breakdown of the expenditure on electricity. Total operational cost of £2.34 million.
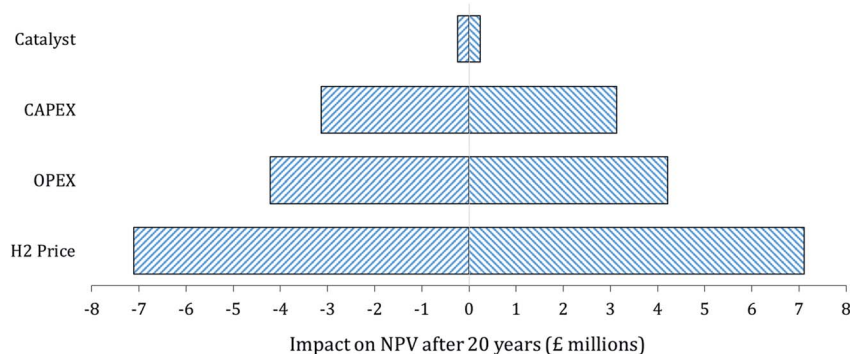

Fig. 9 Difference in NPV (£ millions) after 20 years of operation with ±15% change in labelled factors.

the current (2020) market value of H_2 transport fuel in the UK which is at least £10 per kg. It is, therefore, speculated that the real market value of H_2 should not fall below £4.50 per kg (at pump) for a considerable time. From a global perspective, it is expected the long-term market value will be determined by the cost of large-scale electrolysis and green electricity. If green electricity becomes so cheap that H_2 price drops below £4.50 per kg (at pump) then the OPEX of the discussed process will also drop which would offset some of these proposed losses. Furthermore, if the market value of green electricity is significantly lower than it currently is, it may still be desirable to utilise biogas to produce higher-value products such as H_2 rather than power generation.

Fig. 9 also illustrates that an increase or decrease in OPEX and CAPEX could have a significant impact on the financial attractiveness of process implementation. A 15% increase in OPEX and CAPEX (independently) would delay the achievement of a positive NPV by one and two years respectively; to the 7th and 8th years of operation. As a whole, the sensitivity analysis carried out on the economic study concluded that even with detrimental 15% alterations to various factors, implementation of the process could still be a commercially attractive move for the referenced wastewater treatment plant and thus those with similar characteristics.

7 Results of H_2 production from co-reforming methane and ammonia

Experimental analysis of combined steam methane reforming and ammonia decomposition was carried out to infer the tangible feasibility of the novel process at the core of the model. Table 7 describes the inlet compositions for the experiments and have been separated into categories 1–6. Categories 1–2 have (low) S : C ratios between 2.18–2.32, categories 3–4 have (medium) S : C ratios between 3.24–3.43 and categories 5–6

have (high) S : C ratios between 4.31–4.47. The variation within categories was attributed to slight deviations in methane flows and unavoidable ammonia loss due to volatilisation during sample preparation. Pure SMR experiments are represented in odd numbered categories whilst combined SMR and ammonia decomposition experiments are found in the even numbered categories. The inlet flows in Table 7 were also used for equilibrium modelling for further comparative analysis.

Table 8 displays the results from the analysis of ammonia decomposition from the experiments combining ammonia decomposition and SMR. Ammonia conversions varied from 86 to 98%. Average NH_3 conversions at each temperature analysed (700, 750 and 800 °C) evidenced a positive relationship between temperature and decomposition, as expected from the endothermic nature of reaction (11). As the equilibrium analysis showed >99% conversion of ammonia for each condition experimentally tested, this suggested experimental conditions getting closer to equilibrium of ammonia cracking with increasing reactor temperature. Future tests could be carried

Table 8 Experimental conversion of ammonia *via* decomposition

Run cat	Temp (°C)	NH_3 conversion (%)
2	700	92.5
2	750	91.0
2	800	98.0
4	700	90.2
4	750	86.0
4	800	91.9
6	700	84.9
6	750	91.6
6	800	95.9
Mean	700	89.2
	750	89.5
	800	95.2

Table 7 Flow-rate inlet for experimental runs and equilibrium equivalent

| Run category	Temperature (°C)	CH_4 (mol h⁻¹)	H_2O (mol h⁻¹)	NH_3 (mol h⁻¹)	S : C
1	700	0.049	0.106		2.18
	750	0.048	0.106		2.20
	800	0.047	0.106		2.24
2	700	0.048	0.109	0.007	2.26
	750	0.048	0.112	0.004	2.32
	800	0.048	0.109	0.007	2.29
3	700	0.048	0.159		3.34
	750	0.049	0.159		3.26
	800	0.049	0.159		3.24
4	700	0.048	0.163	0.007	3.39
	750	0.048	0.165	0.005	3.43
	800	0.048	0.165	0.005	3.42
5	700	0.049	0.212		4.33
	750	0.048	0.212		4.38
	800	0.049	0.212		4.33
6	700	0.049	0.218	0.005	4.47
	750	0.050	0.219	0.005	4.41
	800	0.050	0.215	0.008	4.31
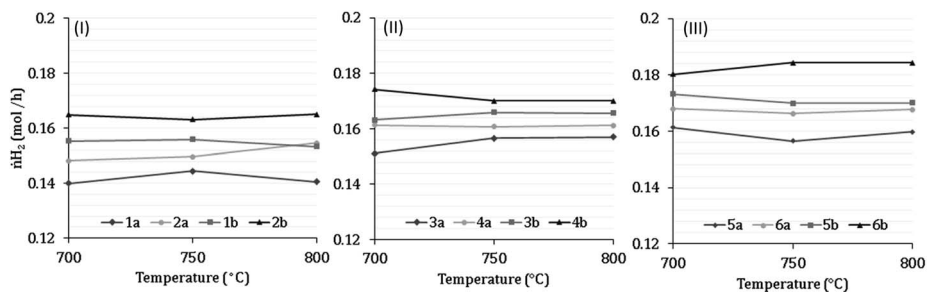
Fig. 10 (I–III). Molar flow (mol h^{-1}) of H$_2$ in product gas from experimental (a) and equilibrium (b) runs. Inlet composition for run categories 1–6 can be found in Table 7.

out using a lower GHSV in order to increase the residence time of gases over the catalyst. General electric suggest a common industry GHSV of 3000 h^{-1}, providing rationale to test lower feed:catalyst ratios.[45]

Fig. 10 to Fig. 13 illustrate the average molar flow rate of H$_2$, CH$_4$, CO and CO$_2$ respectively in the syngas for each experiment alongside their equilibrium equivalent. Fig. 10 (I-III) shows the average H$_2$ flow rate in the product gas under low (I), medium (II) and high (III) S : C conditions respectively. Experimental results from run categories 1 and 2 (low S : C) at 700 °C exhibited the greatest difference in H$_2$ production to equilibrium equivalents at 9.9% and 10.1% lower production rates respectively. The closest H$_2$ production from the experiments got to the equilibrium equivalent was at 800 °C in run categories 3 and 4 (medium S : C) with average H$_2$ flow rates just 5.2% less than their equilibrium equivalent for both categories.

The slightly lower than equilibrium production of H$_2$ can be attributed to the lower rates of SMR, WGS and ammonia decomposition reactions. Fig. 11 demonstrates how the flow of methane in the outlet of each experiment was slightly greater than predicted under equilibrium with the exception of run categories 5 and 6 (high S : C ratios) at 800 °C where the flow of methane was under the micro GC's detectable limit. The experimental data displayed good correspondence with the equilibrium predictions in that methane conversions under the SMR reaction increased with both S : C ratios and temperatures.

The CO flow in the syngas produced during experiments and equilibrium studies can be observed in Fig. 12. With the exception of run category 2 at 700 °C, the flow of CO in the syngas was marginally greater in the experimental product compared to equilibrium, despite having lower rates of SMR. This was the case due to inhibited WGS (reaction 10), the effects
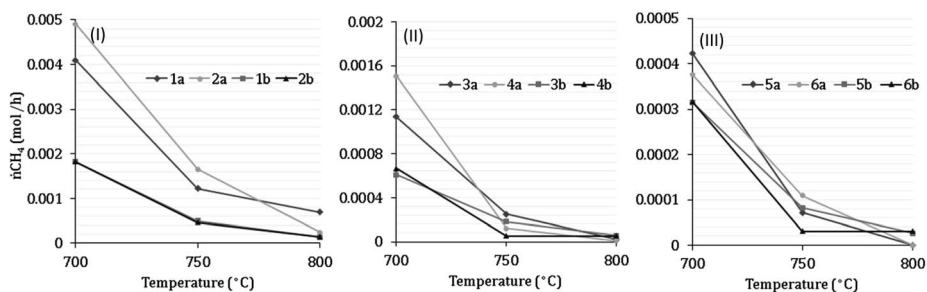

Fig. 11 (I–III). Molar flow (mol h^{-1}) of CH$_4$ in product gas from experimental (a) and equilibrium (b) runs. Inlet composition for run categories 1–6 can be found in Table 7.

Fig. 12 (I–III). Molar flow (mol h^{-1}) of CO in product gas from experimental (a) and equilibrium (b) runs. Inlet composition for run categories 1–6 can be found in Table 7.
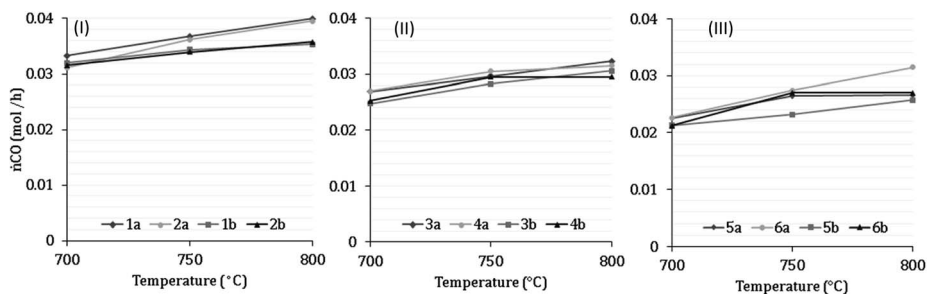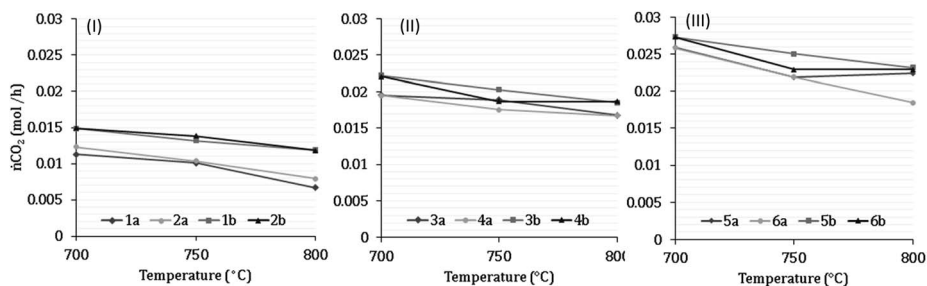
Fig. 13 (I–III). Molar flow (mol h^{-1}) of CO_2 in product gas from experimental (a) and equilibrium (b) runs. Inlet composition for run categories 1–6 can be found in Table 7.
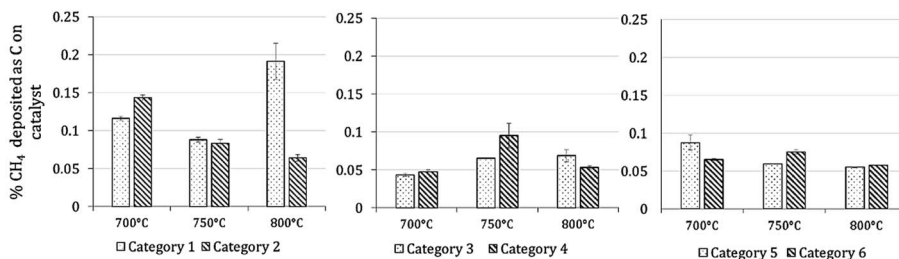

Fig. 14 Carbon deposition as a percentage of inlet methane for run categories 1–6.

of which are also evident when analysing the production of CO_2 in Fig. 13. Experiment syngas CO_2 flows were found to be 24% less than predicted by equilibrium for low S : C but just 4% less for medium S : C. The limited WGS reaction occurring during experiments, therefore had a significant impact on the final yield of H_2.

It was hypothesised *via* equilibrium analysis that the presence of ammonia would have a slight negative impact on the conversion of methane *via* SMR due to the increased flow of H_2 present in the syngas pushing the equilibrium of reaction 9 towards the reactant side. However, this was only found to be the case in just over half of the experiments. It was also hypothesised that carbon deposition would be less pronounced with the introduction of ammonia due to the occupation of acidic sites as discussed by Wang *et al.*[46] However, no obvious correlation could be found, as illustrated in Fig. 14, where less than half of the runs with ammonia demonstrated lower rates of carbon deposition compared to the S : C equivalents without ammonia.

Overall, the data displayed in Fig. 14 shows very little carbon deposition occurred in the experiments carried out. A slight negative correlation between carbon deposition and S : C ratios was found, which is to be expected due to the role of steam in shifting the SMR reaction forwards and mediating the decomposition of methane to solid carbon and H_2 (reaction 16) as the primary route of carbon formation at the investigated temperatures and pressure. For all experiments the carbon deposition was shown on average to be 0.075% of the methane molar flow. For the detailed discussed process, this would equate to 3.4 kg C per day. However, carbon formation is subject to kinetics, process condition and reactor design and these figures may not be representative to real working conditions, especially with the

gap in pressure between the model and experiments.[47] If the catalysts are deactivated *via* carbon formation, they may be regenerated *via* purging with steam or can be replaced altogether.

$$CH_4 \leftrightarrows 2H_2 + C \qquad (16)$$

It has been established that combined ammonia decomposition and SMR can occur in a single packed-bed reactor using a commercial grade nickel catalyst and exhibited good correlation with equilibrium trends. The greater output of CO found experimentally would also help close the gap to equilibrium equivalents in a full H_2 production system, where CO-shift reactors would generate the H_2 proven to originate in the primary reactor under equilibrium. More importantly hardly any carbon deposition was found for operations with co-feeds of ammonia and methane at medium and high S : C. In this sense, the experimental results validate the model data with good confidence. Future work will refine operating conditions with analysis of alternative commercial catalysts, different WHSV/GHVSs to improve the reaction rates of eqn (9)–(11) and a gaseous inlet of ammonia to help control ammonia concentrations and S : C ratios.

Direct translation of the experimental results in the context of the modelling and economic analysis carried out is difficult due to the discussed disparity in exact thermodynamic conditions (model: 1000 °C, 25 bar, reactor: 800 °C, ~1 bar). However, if H_2 generation calculated for the S : C 3 case-study was 5.2% lower, as found with experimental results at atmospheric pressure and a temperature of 800 °C when compared to the equilibrium, a positive NPV would still be achieved during the 8th year of operation, just a year later than in the case-study, and a 20 year NPV 17.6% lower. Given the high discount factor used of 10%, it

can be argued that these are still acceptable numbers for potential investors and wastewater treatment plant operators.

8 Conclusions

To conclude, this work has presented the novel NWaste2H2 process in which ammonia is recovered from digestate liquor produced from anaerobic digestion at an operational wastewater treatment plant for use in a system that generates H_2 *via* a combination of ammonia decomposition and biomethane steam reforming. It was proposed that this H_2 be used as vehicular fuel for fuel cell buses, replacing historically used diesel ones. The ammonia recovery system utilises air stripping, water absorption and distillation to produce a highly concentrated ammonia stream. The modelling of these process steps in Aspen Plus® exhibited a recovery potential of 89.9% which could then be used as a feedstock for H_2 production.

The primary H_2 carrier used in the discussed process is biomethane generated from anaerobic digestion of sewage sludge at the reference WWTP. Modelling of steam methane reforming was performed alongside ammonia decomposition in the system's primary reformer. Three scenarios with different feed molar S : C were simulated and analysed; S : C of 2, 3 and 4 under a reformer pressure 25 bar. As expected, the S : C 4 scenario was capable of the highest methane conversion in the primary reformer at 98.9% compared to 94.8% and 97.9% for S : C scenarios 2 and 3 respectively. The high temperature conditions of the primary reformer (1000 °C) allowed for almost total decomposition of ammonia to H_2 and N_2. High and low temperature WGS reactors were utilised to manipulate the conversion of carbon monoxide to additional H_2. After a PSA separation unit, this resulted in final H_2 production figures of 109.9 kg h^{-1}, 116.1 kg h^{-1} and 118.1 kg h^{-1} for S : C 2, 3 and 4 scenarios respectively.

The price of generating additional H_2 with higher S : C ratios was an increase in heat and power requirements for the system. The heat streams generated were shown to be of insufficient quality to meet the high temperature demands of the air stripper and the distiller. The heat streams would be suitable for space and heat demand for anaerobic digestion at the facility but the quantity of heat available had an inverse relationship with S : C ratios as more heat was required for steam generation and then maintaining temperature in the primary reformer. Power usage had a positive relationship with the S : C ratio with additional electricity required to compress both the reactants and H_2 preparation for dispensing to H_2-fueled buses at 350 bar.

The diversion of ammonia from conventional treatment was predicted to enable a significant drop in GHG emission at 3.2 tonnes CO_2e per day, due to the reduced provision of oxygen required in biological nitrogen removal. Furthermore, GHG emission savings from the use of H_2 as a bus transportation fuel were revealed to be 37 964 kg CO_2e, 39 693 kg CO_2e and 40 790 kg CO_2e per day for S : C 2, 3 and 4 scenarios respectively, with the positive trend occurring due to augmented H_2 generation at higher S : C ratios. This trend was partially offset by the increased emissions attributed to the use of external heat and

power at higher S : C ratios. However, the S : C 4 scenario still demonstrated the highest potential reductions in lifecycle GHG emissions of the three S : C analysed, at 35 414 kg CO_2e per day, equivalent to 17.2 kg per year for each person served by the wastewater treatment plant.

Net present value analysis found that the S : C 3 scenario had also the greatest economic promise with the lower OPEX. For the S : C 3 scenario, an initial total CAPEX of £13.01 million was required and showcased an ability to achieve a positive NPV during the 6th year of operation. Sensitivity analysis demonstrated that the profitability of the process would be highly influenced by the market value of H_2, whereby a 15% drop in the proposed value of H_2 (£4.50 per kg to £3.83 per kg) would lessen the 20 year NPV value by 47%.

A key finding was the heavy influence that compression, storage and dispensing has on the CAPEX and OPEX of the system. In future work, alternative end uses of H_2 will be analysed, such as injection into the UK's National Grid, which has been proposed as a possible option to decrease GHG emissions from the UK heat sector. The feasibility of process implementation at other anaerobic digestion facilities and WWTPs of different scales will also be assessed to interpret the potential role of the discussed process in the UK's energy landscape.

Experimental analysis validated the capability of combining the steam reforming of methane and the decomposition of ammonia in a single packed-bed reactor using a commercial grade 18 wt% $NiO/\alpha\text{-}Al_2O_3$ catalyst. H_2 yields reached between 90–95% of the equilibrium equivalent and ammonia decomposition exhibited higher sensitivity to temperature and steam to carbon ratio with conversions between 86% and 98%. Future work will concentrate on the refining of experimental conditions including analysis of alternative catalysts, and WHSVs, whilst a gaseous flow of ammonia will be used over an aqueous solution to bring more control to the experiments.

Conflicts of interest

There are no conflicts to declare.

Acknowledgements

References

1 I. A. Gondal, S. A. Masood and R. Khan, *Int. J. Hydrogen Energy*, 2018, **43**, 6011–6039.

2 R. Karolyte, *Hydrogen with CCS for decarbonised heat in the Scottish context*, 2017.

3 A. Demirbas, *Energy Sources, Part B*, 2017, **12**, 172–181.

4 N. P. Brandon and Z. Kurban, *Philos. Trans. R. Soc., A*, 2017, **375**, 20160400.

5 E. S. Hanley, J. P. Deane and B. P. Ó. Gallachóir, *Renewable Sustainable Energy Rev.*, 2018, **82**, 3027–3045.

6 G. Maggio, A. Nicita and G. Squadrito, *Int. J. Hydrogen Energy*, 2019, **44**, 11371–11384.

7 A. M. Abdalla, S. Hossain, O. B. Nisfindy, A. T. Azad, M. Dawood and A. K. Azad, *Energy Convers. Manage.*, 2018, **165**, 602–627.

8 M. Reinders, P. Beckhaus, F. Illing, U. Misz, H. Riße, M. Schröder, P. Schulte and B. Teichgräber, *Int. J. Hydrogen Energy*, 2015, **40**, 8601–8606.

9 H. J. Alves, C. Bley Junior, R. R. Niklevicz, E. P. Frigo, M. S. Frigo and C. H. Coimbra-Araújo, *Int. J. Hydrogen Energy*, 2013, **38**, 5215–5225.

10 S. Hwangbo, K. J. Nam, J. Han, I. B. Lee and C. K. Yoo, *Energy Trends*, 2018, **140**, 386–397.

11 Department for Business Energy & Industrial Strategy, *National Statistics*, DOI: 10.4324/9780203732861-2.

12 C. Vaneeckhaute, V. Lebuf, E. Michels, E. Belia, P. A. Vanrolleghem, F. M. G. Tack and E. Meers, *Waste Biomass Valorization*, 2016, 1–20.

13 M. Errico, L. Fjerbaek Sotoft, A. Kjærhuus Nielsen and B. Norddahl, *Clean Technol. Environ. Policy*, 2017, **20**, 1479–1489.

14 Agriculture and Horticulture Development Board (AHDB), *GB Fertiliser Price Market Update Monthly average prices for June 2020 GB Fertiliser Price Market Update*, 2020.

15 O. Grasham, V. Dupont, M. A. Camargo-Valero, P. García-Gutiérrez and T. Cockerill, *Appl. Energy*, 2019, **240**, 698–708.

16 CEC – Council of the European Communities, *Off. J. Eur. Communities: Legis.*, 1991, **135**, 40–52.

17 CEC – Council of the European Communities, *Off. J. Eur. Communities: Legis.*, 2000, **327**, 1–72.

18 J. M. Garrido, M. Fdz-Polanco and F. Fdz-Polanco, *Water Sci. Technol.*, 2013, **67**, 2294.

19 M. J. Kampschreur, H. Temmink, R. Kleerebezem, M. S. M. Jetten and M. C. M. van Loosdrecht, *Water Res.*, 2009, **43**, 4093–4103.

20 J. Andrews, B. Chambers, A. Davey, S. Galetti, J. Hobson, D. Hunt, R. Thorman and I. Walkerm, *Carbon Accounting in the Water Industry; non-CO_2 Emissions*, UKWIR, London, 2009.

21 V. Parravicini, K. Svardal and J. Krampe, *Energy Procedia*, 2016, **97**, 246–253.

22 R. Berger, *Fuel Cell Electric Buses – Potential for Sustainable Public Transport in Europe FCH JU – Commercialisation Strategy for Fuel Cell Electric Buses in Europe*, 2015.

23 B. Roland, *Fuel Cells and Hydrogen for Green Energy in European Cities and Regions*, 2018.

24 The Hydrogen Council, *Path to hydrogen competitiveness a cost perspective*, 2020.

25 IEA, *Hydrogen*, Paris, 2020.

26 V. Willmann, *LowCVP Low Emission Bus Workshop*, Glasgow, 08/03/2018.

27 C. Hatch, A. Center, A. S. Feitelberg, E. M. Fisher and P. F. Mutolo, *Int. J. Hydrogen Energy*, 2013, **38**, 16002–16010.

28 Department of Business Energy & Industrial Strategy, *2019 Government greenhouse gas conversion factors for company reporting: Methodology paper*, London, 2019.

29 *Aspen Plus*, Aspen Technology, 2017.

30 AWWA, in *Standard methods for the examination of water and wastewater*, 1999.

31 G. Mininni, G. Laera, G. Bertanza, M. Canato and A. Sbrilli, *Environ. Sci. Pollut. Res. Int.*, 2015, **22**, 7203–7215.

32 N. Hill, E. Bonifazi, R. Bramwell, B. Karagianni and B. Harris, *Government GHG Conversion Factors For Company Reporting: Methodology paper for emission factors: final report*, 2018, p. 141.

33 Department for Business Energy & Industrial Strategy, *2019 Government Greenhouse Gas Conversion Factors for Company Reporting: Methodology Paper for Emission Factors Final Report*, Stationary Office, London, 2019.

34 Department of Business Energy & Industrial Strategy, *Updated Energy and Emissions Projections 2017*, London, 2018.

35 Parliamentary Office of Science and Technology, *Carbon Footprint of Heat Generation*, 2016, vol. 523.

36 Aspen Technology, *Aspen Plus Economic Analyzer*, 2017.

37 M. Penev, G. Saur, C. Hunter and J. Zuboy, *H2A Hydrogen Production Model: Version 3. 2018 User Guide (DRAFT)*, 2018.

38 M. S. Peters, K. D. Timmerhaus and R. E. West, in *Plant design and economics for chemical engineers*, McGraw-Hill, New York, 5th edn, 2004, pp. 642–754.

39 L. Kaiwen, Y. Bin and Z. Tao, *Energy Sources, Part B*, 2018, **13**, 109–115.

40 B. Reuter, M. Faltenbacher, O. Schuller, N. Whitehouse and S. Whitehouse, *New Bus ReFuelling for European Hydrogen Bus Depots: High-Level Techno-Economic Project Summary Report*, 2017.

41 Department of Business Energy & Industrial Strategy, *Gas and electricity prices in the non-domestic sector*, 2018.

42 W. A. Alkhayat and A. M. Gerrard, in *Transactions of the American Association of Cost Engineers (Trans Am Assoc Cost Eng Annu Meet)*, Montreal, Canada, 1984, pp. 1.2.1–1.2.4.

43 R. Turton, R. C. Bailie, W. B. Whiting and J. A. Shaeiwitz, in *Analysis, Synthesis, and Design of Chemical Processes*, ed. R. Turton, R. C. Bailie, W. B. Whiting and J. A. Shaeiwitz, Prentice Hall, Upper Saddle River, N.J., 3rd edn, 2008.

44 The United Kingdom Department of Transport, *Renewable Transport Fuel Obligation Guidance Part One Process Guidance Moving Britain Ahead*, London, 2018.

45 W. Wei and K. Liu, *presented at the 2007 Bio-Derived Liquids to Hydrogen Distributed Reforming Working Group held November 6, 2007 in Laurel, Maryland*, GE Global Research, DOI: 10.1017/CBO9781107415324.004.

46 W. Wang, R. Ran, C. Su, Y. Guo, D. Farrusseng and Z. Shao, *J. Power Sources*, 2013, **240**, 232–240.

47 J. N. Armor, *Appl. Catal., A*, 1999, **176**, 159–176.